THE GRADIENT OF TOTAL MULTIPLE SCATTERING CROSS SECTION AND ITS APPLICATION TO ACOUSTIC CLOAKING

FERUZA A. AMIRKULOVA

Mechanical Engineering, San Jose State University, San Jose, CA 95192, USA feruza.amirkulova@sjsu.edu

ANDREW N. NORRIS

Mechanical and Aerospace Engineering, Rutgers University, Piscataway, NJ 08854-8058, USA norris@rutgers.edu

We derive a formula for the gradients of the total scattering cross section (TSCS) with respect to positions of a set of cylindrical scatterers. The analytic form enhances modeling capability when combined with optimization algorithms and parallel computing. As application of the method we consider a gradient-based minimization of TSCS for a set of cylindrical obstacles by incrementally repositioning them so that they eventually act as an effective cloaking device. The gradient-based optimization algorithm reduces the TSCS by evaluating its derivative with respect to the cylinder positions and then perturbatively optimizing the position of each cylinder in the cloaking device while taking into account acoustic multiple scattering between the cylinders. The method is illustrated for clusters of hard cylinders and sets of elastic thin shells in water.

Keywords: acoustics, scattering, total scattering cross section, gradient based optimization, cloaking

1. Introduction

An acoustic cloak renders an object invisible to incident waves. There are two types of acoustic cloak, namely, passive ^{1,2,3} and active ⁴. Here, we consider passive mechanisms, and propose a semi-direct method for cloaking design using gradient-based optimization algorithms. In particular we demonstrate how the analytical form of gradients of the objective function improves the accuracy of the optimized solution. Passive cloaking can be achieved using metamaterials with the acoustic anisotropy required by Transformation Acoustics ^{1,2,3}. Here, however, we seek more limited cloaking for a limited incidence direction at a single frequency and band of frequencies by minimizing the scattering of a given cluster of scatterers. This can indeed be achieved with an appropriate arrangement of the targets. If one allows for rearrangement then the same cluster can operate at different, although unique, frequencies.

In the first study in this area Garcia-Chocano et al. ⁵ proposed an inverse design of a 2D acoustic cloak for airborne sound using a multiple scattering (MS) theory and non-gradient optimization technique combining genetic algorithms (GA) and simulated annealing (SA). They ⁶ further designed a 3D axisymmetric cloak and demonstrated the cloaking performance experimentally. They had previously used MS theory and GA in inverse design of

photonic crystals ⁷ and flat acoustic lenses ^{8,9}. Romero-García et al. ¹⁰ studied the optimization of the attenuation and focusing of phononic crystal arrays resulting from the deliberate creation of holes using multiobjective evolutionary algorithm and MS theory. Gao et al. ¹¹ presented a dual-layer acoustic cloak made up of homogeneous single-negative medium using genetic algorithm. The parallelized version of genetic algorithms was also used by Serna et al. ¹² to design a multilayer homogeneous dielectric filler for electromagnetic invisibility based on plasmonic cloaking.

Andkjær and Sigmund ^{13,14,15} designed a topology-optimized acoustic cloak that conceals an aluminum cylinder from airborne sound using a gradient-based topology optimization algorithm and FEM analysis; they also studied the dependency of cloaking performance on the incidence angle, and designed a broadband cloak by optimizing it at three frequencies. Lin et al. ¹⁶ also designed a broadband acoustic cloak using the gradient-based topology optimization. Diest ¹⁷ has discussed and reviewed optical metamaterial designs using gradient free optimization such as direct methods, surrogate models, stochastic search algorithms as well as gradient based optimization methods using level set method based on shape and/or topological derivatives. Arridge and Schweiger ¹⁸ derived optical tomography schemes using non-linear optimization and FEM analysis; they demonstrated a simple means to obtain the gradient of the objective function directly, and applied gradient-based optimization based on Newton-like methods. Amirkulova et al. ¹⁹ presented a gradient-based optimization of pressure amplitude at the focal point to design an acoustic lens. Blankrot and and Heitzinger ²⁰ presented a gradient based optimization of dielectric metamaterial devices by means of MS theory and FMM using Nyström discretization for a single prototype inclusion. However, they ²⁰ did not provide explicit analytical formulas for the gradients of the objective function. Kalantari and Bakr ²¹ proposed 2D and 3D electric cloaks of arbitrarily shaped objects using steepest descent approach with line search where the gradients were supplied by an adjoint variable method. Chen et al. ²² used the gradient descent method to solve different material design optimization problems; they discussed both eigenfunction optimization and level sets optimization algorithms, and demonstrated the robustness of the gradient based approach with numerical results. Ronellenfitsch et al. ²³ presented the spectral optimization of a set of spring stiffnesses in the unit cell to control the appearance and number of band-gaps in the vibrational spectrum of an acoustic spring network. Peralta and Fachinotti ²⁴ designed heat flux manipulation devices for heat concentration and a cloak using a Discrete Material Optimization method and IPOPT software. However, a cloak design using the analytical form of the gradients of the pertinent objective function has not yet been shown. Fachinotti et al. ²⁵ also used the Discrete Material Optimization technique and the finite element method to design elastostatic cloaking device by solving a nonlinear optimization problem where the objective function defines the error in matching a desired displacement field.

One of the advantages of using stochastic global optimization is that these methods do not require the evaluation of the gradient of the objective function. However, when the analytical form of the gradient is available, it can be used to improve the numerical performance of stochastic optimization enhancing the quality and precision of global optimal solution ^{26,27}. The accuracy of solutions obtained with gradient-based optimization algorithms ^{26,27} exceed those obtained with traditional stochastic algorithms such as GA and SA. In addition, non-gradient optimization algorithms require orders of magnitude more function evaluations than is required for gradient based optimization approaches ²⁸.

In this work, we obtain a semi-analytical formula for the gradient of the Total Scattering Cross Section (TSCS) with respect to cylinder positions. We combine these formulae with gradient-based optimization algorithms and apply them to design a directional acoustic cloak that conceals a ring of rigid cylinders (or elastic shells) submerged in water. This enhances optimization studies by allowing the use of exact gradients with optimization algorithms and parallel computing, reducing the number of function calls, time to converge ²⁹, and improving the solution accuracy on large scales, especially at high frequencies and for a large number of scatterers. As example application, we consider the minimization of TSCS that leads to cloaking designs for acoustic waves for a given incident plane wave. The acoustic cloaking device is achieved by optimizing the spatial placement and distribution of the scatterers in the acoustic medium. The location and distribution of the cylinders (shells) are optimized such that their combined scattering pattern cancel the scattering from a cylinder or a configuration of cylinders located inside the cloaked region. Here, we study how efficiently objects can be cloaked when using rigid cylinders and thin cylindrical shells made of conventional simple isotropic materials readily available in nature.

The paper is organized as follows. Section 2 begins with a definition of the multiple scattering problem and the position dependent total scattering cross section. Gradients of the TSCS with respect to the scatterer positions are then obtained by means of MS theory ³⁰ and by employing the optical theorem. Some properties of the gradient vectors are illustrated through numerical examples in Section 32.5. Application of the closed form for the TSCS gradient to acoustic cloaking are given in Section 3.2. Single frequency and broadband cloaking are illustrated using multiple reconfigurable cylinders as the cloaking mechanism.

2. Problem definition

We consider multiple scattering in the context of the acoustic time harmonic wave equation in two dimensions. Time harmonic dependence $e^{-i\omega t}$ is assumed but omitted in the following. The governing equation for the acoustic pressure $p(\mathbf{x})$, $\mathbf{x} \in \mathbb{R}^2$, is the Helmholtz equation

$$\nabla^2 p + k^2 p = 0, (2.1)$$

where $k = \omega/c$ is the wavenumber, c is the acoustic speed, and ω is the frequency. The total field $p(\mathbf{x})$ is defined as the sum of incident p_{inc} and scattered p_{sc} pressure fields:

$$p = p_{inc} + p_{sc}. (2.2)$$

The incident field is a plane wave which interacts with a given configuration of Mseparate scatterers. For simplicity, we take these to be circularly cylindrical scatterers, which

4 Amirkulova and Norris

may be either rigid cylinders or thin elastic shells. Our objective is to reduce the scattering by rearranging the scatterers. As a measure of the scattering we use total scattering cross section (TSCS). The critical quantity that we use in the process is the gradient of the TSCS, defined next.

2.1. Gradient of the scattering cross section

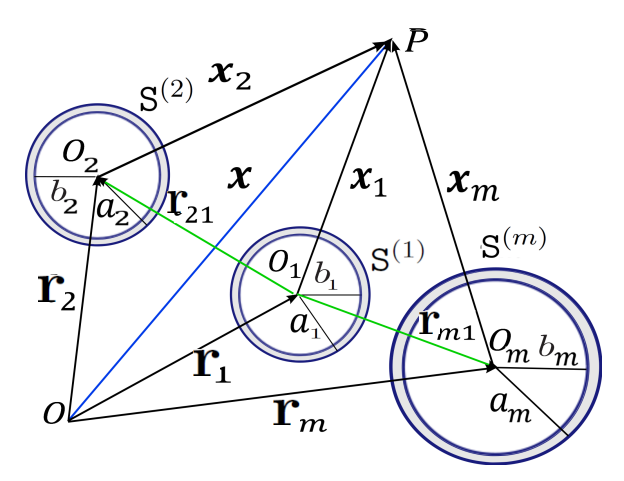


Fig. 1: An arbitrary planar configuration of M cylinders \mathbb{S}_m with outer radius a_m and inner radius b_m , $m = \overline{1, M}$.

Let σ denote the total scattering cross section. For a single cylinder, σ is obviously independent of the position of the scatterer. For a pair of cylinders, the TSCS depends on the relative positions, $\sigma = \sigma(\mathbf{r}_1 - \mathbf{r}_2)$, where the vectors \mathbf{r}_1 , \mathbf{r}_2 define the cylinder centers shown in Fig. 1. For M cylinders, we have dependence on M-1 relative position vectors, e.g.

$$\sigma = \sigma(\mathbf{r}_1 - \mathbf{r}_2, \mathbf{r}_1 - \mathbf{r}_3, \mathbf{r}_1 - \mathbf{r}_4, \cdots, \mathbf{r}_1 - \mathbf{r}_M). \tag{2.3}$$

This redundancy has the following physical implication. Define the gradient vectors

$$\mathbf{s}_j = \frac{\partial \sigma}{\partial \mathbf{r}_j}, \quad j = 1, 2, \dots M.$$
 (2.4)

If scatterer j is moved incrementally by $\Delta \mathbf{r}_j$ the associated change in the TSCS is

$$\Delta \sigma = \sum_{j=1}^{M} \mathbf{s}_j \cdot \Delta \mathbf{r}_j. \tag{2.5}$$

However, if all the scatterers are shifted (translated) the same amount, $\Delta \mathbf{r}_j = \Delta \mathbf{r}$ for all j, then σ cannot change, i.e. $\Delta \sigma = 0$. Since the direction of $\Delta \mathbf{r}$ is arbitrary it implies

$$\sum_{j=1}^{M} \mathbf{s}_j = 0. \tag{2.6}$$

This single relation for the M gradient vectors \mathbf{s}_j is a consequence of translation invariance. It can also be seen as a result of direct differentiation of eq. (2.3).

2.2. Total scattering cross-section

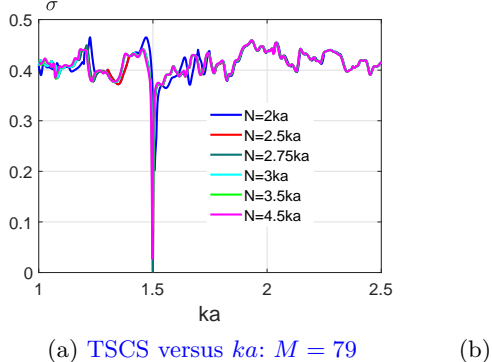
The total scattering cross-section is directly related by the optical theorem to the scattering amplitude in the forward direction, i.e. the direction of propagation of the incident plane wave, here assumed to be \mathbf{e}_1 or the x-direction. Thus 31

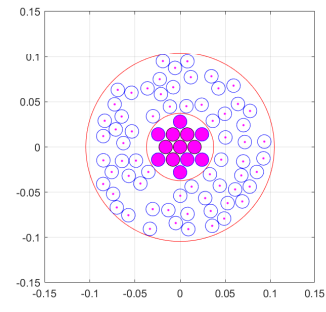
$$\sigma = -2\operatorname{Re} f(0). \tag{2.7}$$

where the far-field amplitude form function, $f(\theta) = f(\theta, \mathbf{r}_1, \mathbf{r}_2, \dots, \mathbf{r}_M)$, $\theta = \arg(\mathbf{x})$, is defined by the scattered pressure p^{sc} in the far-field by eq. (A.16). Thus,

$$\sigma = -\frac{4}{k} \operatorname{Re} \sum_{n=-\infty}^{\infty} \sum_{m=1}^{M} (-i)^n e^{-i k x_m} B_n^{(m)}$$
 (2.8)

where $x_m = \mathbf{e}_1 \cdot \mathbf{r}_m$. Let N be the truncation value of the infinite sum in eq. (2.8) chosen so that the TSCS is well approximated. In practice, the value of N depends upon frequency, but typically $N \approx 2.5ka$ is adequate, see Figure 2(a).





(b) Optimized configuration: M = 79

Fig. 2: Variation of TSCS versus non-dimensional wavenumber ka at different values of mode order truncation, N, with $\frac{N}{ka} = 2$; 2.5; 2.75; 3; 3.5; 4.5 for a configuration optimized at ka = 1.5 with M = 79 scatterers of radii a = 0.0075m, and depicted in Figure 2(b); the optimization process is described in Section 3.2.

Introduce the vectors $\mathbf{a}, \mathbf{b} \in \mathcal{C}^{M \times (2N+1)}$. The components of the scattering coefficient vector $\mathbf{b} = \{B_n^{(j)}\}, j \in (1, M), n \in (-N, N), \text{ are } B_n^{(j)} = \{B_n(\mathbf{r}_j)\} \text{ from eq. (2.8). The elements of the dual vector } \mathbf{a} = \{A_n^{(j)}\} = \{A_n(\mathbf{r}_j)\} \text{ are } A_n^{(m)} = A_n(\mathbf{r}_m) = \mathbf{i}^n e^{\mathbf{i} k x_m}, \text{ such } \mathbf{a} \in \{A_n^{(j)}\} = \{A_n(\mathbf{r}_j)\} \text{ are } A_n^{(m)} = A_n(\mathbf{r}_m) = \mathbf{i}^n e^{\mathbf{i} k x_m}, \mathbf{a} \in \{A_n^{(j)}\} = \{A_n^{(j)}\} \text{ are } A_n^{(m)} = A_n^{(m)} = \mathbf{i}^n e^{\mathbf{i} k x_m}, \mathbf{a} \in \{A_n^{(m)}\} = \{A_n^{(m)}\} =$

that

$$\mathbf{a} = \begin{pmatrix} \mathbf{a}^{(1)} \\ \mathbf{a}^{(2)} \\ \vdots \\ \mathbf{a}^{(M)} \end{pmatrix}, \quad \mathbf{b} = \begin{pmatrix} \mathbf{b}^{(1)} \\ \mathbf{b}^{(2)} \\ \vdots \\ \mathbf{b}^{(M)} \end{pmatrix}, \quad \mathbf{a}^{(j)} = \begin{pmatrix} A_{-N}^{(j)} \\ A_{-N+1}^{(j)} \\ \vdots \\ A_{N}^{(j)} \end{pmatrix}, \quad \mathbf{b}^{(j)} = \begin{pmatrix} B_{-N}^{(j)} \\ B_{-N+1}^{(j)} \\ \vdots \\ B_{N}^{(j)} \end{pmatrix}. \tag{2.9}$$

The TSCS can then be expressed

$$\sigma = -\frac{4}{k} \operatorname{Re} \mathbf{a}^{\dagger} \mathbf{b} \tag{2.10}$$

where \mathbf{a}^{\dagger} is the Hermitian transpose.

2.3. The scattering vector b

The column vector \mathbf{b} satisfies the relation

$$X \mathbf{b} = \mathbf{a}, \tag{2.11}$$

where X is the interaction matrix that defines the coupling between each scatterer of the configuration (see Appendix A for details)

$$\mathbb{X} = \begin{bmatrix} \mathbf{T}^{(1)^{-1}} & -\mathbf{P}^{1,2} & -\mathbf{P}^{1,3} & \cdots & -\mathbf{P}^{1,M} \\ -\mathbf{P}^{2,1} & \mathbf{T}^{(2)^{-1}} & -\mathbf{P}^{2,3} & \cdots & -\mathbf{P}^{2,M} \\ \vdots & \vdots & \vdots & \ddots & \vdots \\ -\mathbf{P}^{M,1} & -\mathbf{P}^{M,2} & -\mathbf{P}^{M,3} & \cdots & \mathbf{T}^{(M)^{-1}} \end{bmatrix}.$$
 (2.12)

Here $\mathbf{T}^{(j)}$ is the transition or T-matrix for scatterer j, and $\mathbf{P}^{j,m} = \begin{bmatrix} \mathbf{P}_{ql}^{j,m} \end{bmatrix}$ is a Toeplitz matrix that depends on the position vector \mathbf{r}_{jm} depicted in Figure 1. The matrix $\mathbf{P}^{j,m}$ takes into account the interaction between the scatterers, whereas the transition matrix $\mathbf{T}^{(j)}$ depends on the shape and the physical properties of the material of cylinder, as well as the boundary conditions on the interfaces.

The matrix X and its inverse is represented by four-indices, satisfying

$$\sum_{i=1}^{M} \sum_{n=-\infty}^{\infty} X_{pqin}^{-1} X_{inml} = \sum_{i=1}^{M} \sum_{n=-\infty}^{\infty} X_{pqin} X_{inml}^{-1} = \delta_{pm} \delta_{ql}.$$
 (2.13)

Here we consider 2-dimensional configurations of circularly cylindrical scatterers, for which the T-matrices become diagonal, see 32 for specific details. In particular, $\mathbf{P}^{j,m} = \begin{bmatrix} P_{ql}^{j,m} \end{bmatrix}$ for $j,m \in (1,M), j \neq m, l,q \in (-N,N)$,

$$P_{ql}^{j,m} = P_{ql}(\mathbf{r}_{jm}) = H_{l-q}^{(1)}(kr_{jm})e^{i(l-q)\arg\mathbf{r}_{jm}}$$
(2.14)

where $\mathbf{r}_{jm} = \mathbf{r}_j - \mathbf{r}_m$ and $H_n^{(1)}$ is the Hankel function of the first kind of order n.

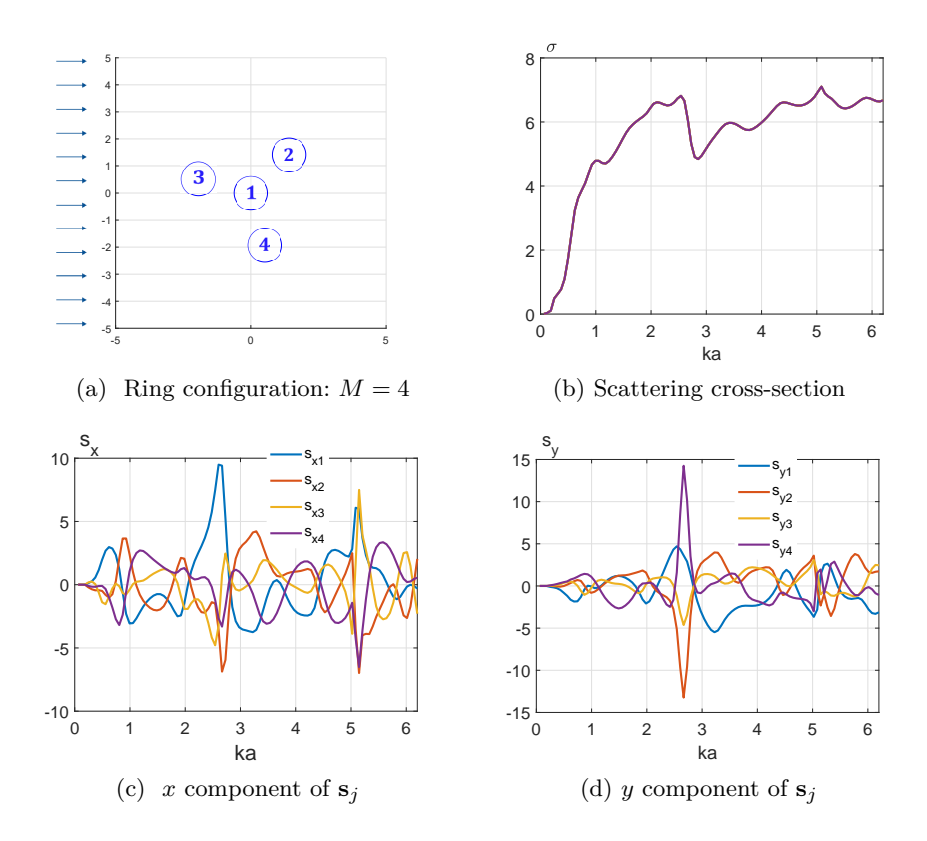


Fig. 3: Variation of components of the gradient vector with non-dimensional wavenumber for a configuration of M=4 rigid cylinders that is non-symmetric with respect to the x and y axes.

2.4. Explicit form of the gradient vector s_i

The TSCS follows from (2.10) and (2.11) as

$$\sigma = -\frac{4}{k} \operatorname{Re} \mathbf{a}^{\dagger} \mathbb{X}^{-1} \mathbf{a}. \tag{2.15}$$

This expression for σ , combined with the definition (2.4) will be used to find the gradient of the TSCS. A critical simplification in the process is that the T-matrices are independent of the scatterer positions. This is true not only for the circularly symmetric scatterers considered here but more generally since the T-matrix is translation invariant. However, in the more general case of non-circularly symmetric scatterers one can also define gradients with respect to scatterer orientation, which are identically zero in the present case. Noting that $\frac{\partial \mathbb{X}^{-1}}{\partial \mathbf{r}} = -\mathbb{X}^{-1} \frac{\partial \mathbb{X}}{\partial \mathbf{r}} \mathbb{X}^{-1}$, the vector \mathbf{s}_j may be written as

$$\mathbf{s}_{j} = -\frac{4}{k} \operatorname{Re} \left[\frac{\partial \mathbf{a}^{\dagger}}{\partial \mathbf{r}_{i}} \mathbf{b} + \mathbf{a}^{\dagger} \mathbb{X}^{-1} \left(\frac{\partial \mathbf{a}}{\partial \mathbf{r}_{i}} - \frac{\partial \mathbb{X}}{\partial \mathbf{r}_{i}} \mathbf{b} \right) \right]. \tag{2.16}$$

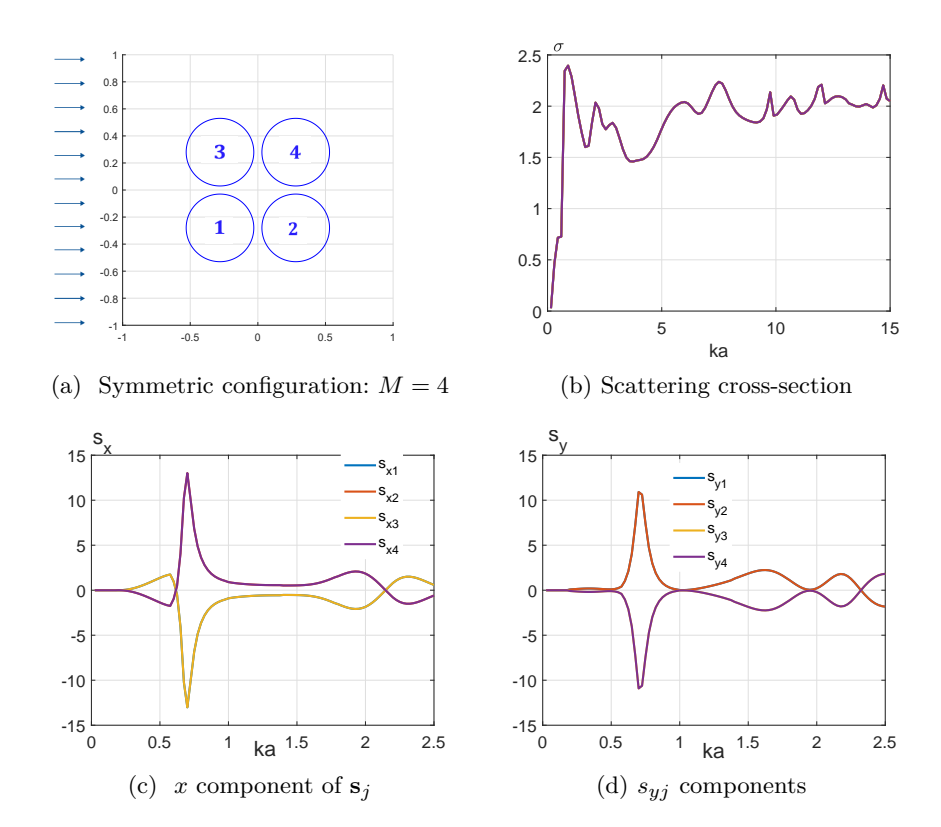


Fig. 4: Variation of components of a gradient vector, \mathbf{s}_j , with ka for a symmetric configuration of M=4 rigid cylinders. Here $s_{x1}=-s_{x2}=s_{x3}=-s_{x4}$ and $s_{y1}=s_{y2}=-s_{y3}=-s_{y4}$.

Based on the fact that the T-matrices are independent of position, the gradient of the components of the matrix X are

$$\frac{\partial X_{inml}}{\partial \mathbf{r}_{j}} = \begin{cases} O_{nl} \delta_{ij}, & i = m, \\ \delta_{jm} \frac{\partial P_{nl}}{\partial \mathbf{r}_{j}} (\mathbf{r}_{ji}) - \delta_{ji} \frac{\partial P_{nl}}{\partial \mathbf{r}_{j}} (\mathbf{r}_{jm}), & i \neq m, \end{cases}$$
(2.17)

where O_{nl} are components of the zero matrix. The gradients in eq. (2.17) follow from

$$\frac{\partial P_{nl}}{\partial \mathbf{r}_j}(\mathbf{r}_{jm}) = \frac{k}{r_{jm}} V_{l-n}^{+\prime}(\mathbf{r}_{jm}) \,\mathbf{r}_{jm} + \frac{\mathrm{i}(l-n)}{r_{jm}^2} V_{l-n}^{+}(\mathbf{r}_{jm}) \,\mathbf{e}_3 \times \mathbf{r}_{jm},\tag{2.18}$$

where V_n^+ and the derivative function $V_n^{+\prime}$ are defined as

$$V_n^+(\mathbf{x}) = H_n^{(1)}(k|\mathbf{x}|)e^{i n \arg \mathbf{x}}, \quad V_n^{+'}(\mathbf{x}) = H_n^{(1)\prime}(k|\mathbf{x}|)e^{i n \arg \mathbf{x}}.$$
 (2.19)

The gradient of the components of **a** with respect to the position of the *j*-th scatterer is $\partial \mathbf{a}^{(m)}/\partial \mathbf{r}_j = \delta_{jm} \mathbf{a}^{(m)} \otimes \mathrm{i} k \, \mathbf{e}_1 \in \mathcal{C}^{M \times (2N+1)} \times \mathcal{C}^2$. Finally, eq. (2.16) can be written in

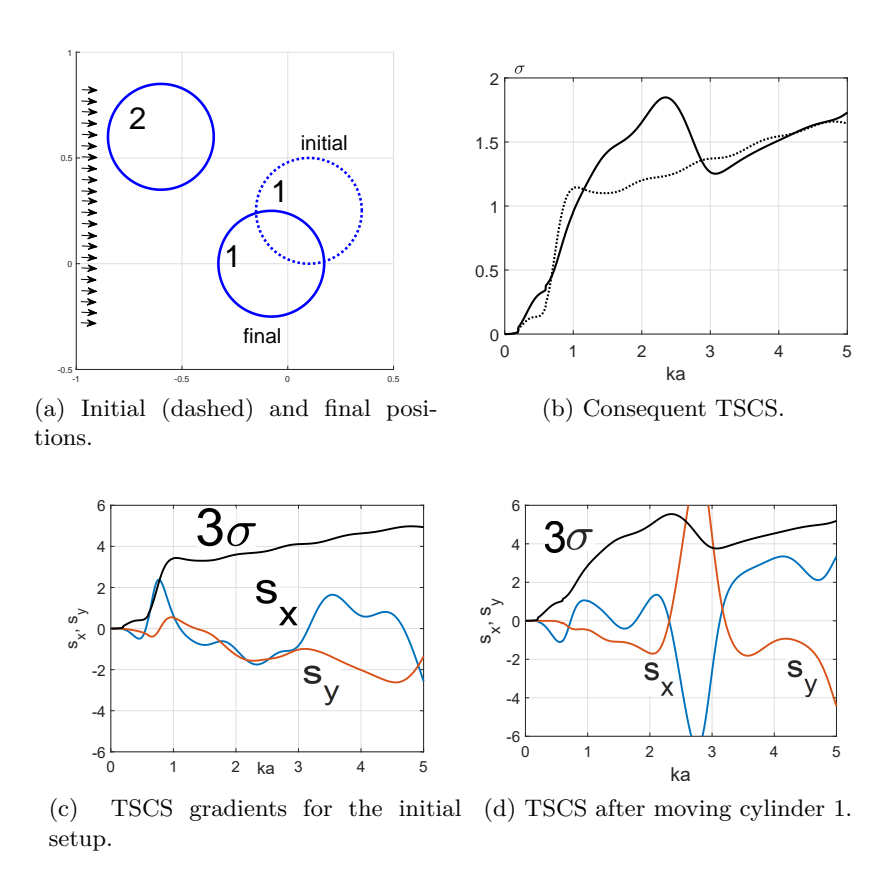


Fig. 5: Knowledge of the gradient provides a way to increase TSCS in a frequency range where it does not display a local maximum. The initial and final TSCS are compared in (b). Note that the displacement in (a) also produces a local minimum at about ka = 3. The almost zero gradients in (d) verify the local minimum and maximum.

component form as

$$\mathbf{s}_{j} = -\frac{4}{k} \operatorname{Re} \sum_{m=1}^{M} \sum_{l=-\infty}^{\infty} \left[\frac{\partial A_{l}^{*}(\mathbf{r}_{m})}{\partial \mathbf{r}_{j}} B_{l}^{(m)} + A_{l}^{*}(\mathbf{r}_{m}) \sum_{i=1}^{M} \sum_{n=-\infty}^{\infty} (X^{-1})_{lmin} \right] \times \left(\frac{\partial A_{n}(\mathbf{r}_{i})}{\partial \mathbf{r}_{j}} - \sum_{p=1}^{M} \sum_{q=-\infty}^{\infty} \frac{\partial X_{inpq}}{\partial \mathbf{r}_{j}} B_{q}^{(p)} \right) , \quad j \in (1, M).$$

$$(2.20)$$

2.5. Numerical examples

The gradient \mathbf{s}_j has some interesting features that will be presented before considering the cloaking problem. Figure 3 considers a configuration of four rigid cylinders that is not symmetric with respect to the x and y axes. The numerical results show that while the s_{xj} and s_{yj} components have different values, the sum of all four components vanishes at every

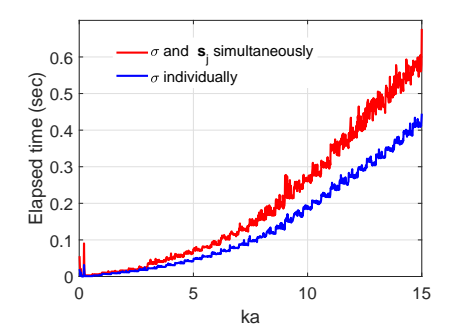


Fig. 6: The elapsed time spent in seconds for the sequential evaluation of TSCS, σ , and a gradient vector, \mathbf{s}_j , with respect to wavenumber ka for a symmetric configuration of M=4 rigid cylinders depicted in Figure 4 (a). The blue curve corresponds to elapsed time spent for the individual evaluation of σ , and the red curve corresponds to the concurrent evaluation of σ and gradient vectors \mathbf{s}_i evaluated at 1000 discrete values of $ka \in (0, 15]$.

value of ka: $\sum_{j=1}^4 s_{xj} = 0$ and $\sum_{j=1}^4 s_{yj} = 0$. Geometrical symmetry, such as the four rigid cylinders in Figure 4, implies corresponding symmetry conditions on the gradient vectors. In this case $s_{x1} = s_{x3}$, $s_{x2} = s_{x4}$, which, combined with the fact that $\sum_{j=1}^4 s_{xj} = 0$, means that there is only one independent s_{xj} . The y-components satisfy the geometrical identities $s_{y1} = -s_{y3}$ and $s_{y2} = -s_{y4}$, but since these already guarantee that $\sum_{j=1}^4 s_{yj} = 0$ the latter does not provide any further information. However, one can use a different argument to again show that there is only a single independent component. Consider the incident wave as the sum of two fields: one comprising a wave from the left and a wave from the right of equal amplitude, the other as two waves of opposite amplitude. These fields are symmetric/antisymmetric about the y- and for each we see that $s_{y1} = s_{y2}$ and $s_{y3} = s_{y4}$. In summary: $s_{x1} = -s_{x2} = s_{x3} = -s_{x4}$ and $s_{y1} = s_{y2} = -s_{y3} = -s_{y4}$.

Figure 5 illustrates a simple application of the gradient vector for maximizing the scattering cross-section. For a given initial configuration of two rigid cylinders the cross-section for $ka \leq 2.5$ is as shown in Fig. 5c. The large gradient at approximately ka = 2.25 indicates that slight relative movement of cylinder 1 could significantly effect the TSCS. Since both components are negative and approximately equal, this suggests displacing the rigid cylinder as shown in Fig. 5a. The resulting TSCS is compared with the original in Fig. 5b, and Fig. 5d now shows zero gradient at $ka \approx 2.25$, indicating a local maximum in TSCS.

Figure 6 illustrates the elapsed time for the sequential evaluation of TSCS function, σ , and gradient vectors \mathbf{s}_j as compared with the time taken for σ alone. There is an additional cost for the gradient evaluation but this cost is compensated during the optimization process when combined with parallel computation. Providing the gradients allows the solver to converge faster and provide more accurate results. For example, for a multiring configuration of thin elastic shells with M=79 and ka=0.15, using 4 CPUs on MacbookPro with 16GB of RAM and providing the gradients reduced the total compute time for one optimization simulation from 17.58 hours to 0.57 hours while improving the accuracy from 1.681e-07

to 1.145e - 07.

3. Minimizing scattering cross-section: acoustic cloaking

For given scatterer location points the gradients \mathbf{s}_j are in the direction of greatest increase of TSCS. As seen in the example of Figure 5 this provides the optimal directions to increase TSCS by incremental displacement. In contrast, in order to minimize the TSCS of cloaking annulus we will move the cylinders in the annulus in the direction opposite to the gradient vectors, i.e. $-\mathbf{s}_j$. This is achieved in MATLAB with the use of Global Optimization and Parallel Computing Toolboxes, and by supplying the derived analytic form of the gradients vectors from eq. (2.20).

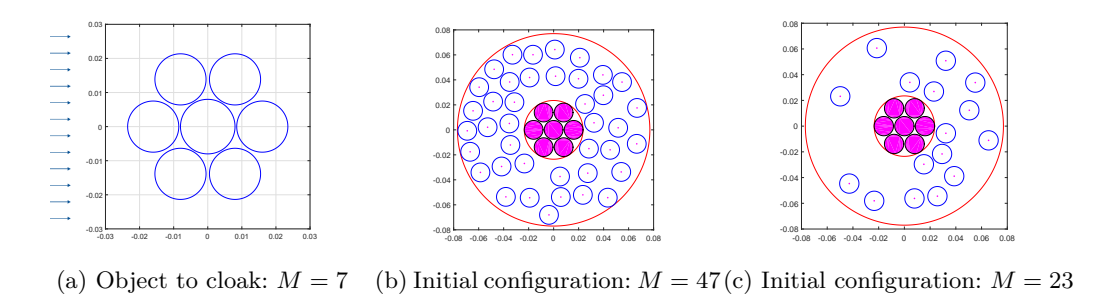


Fig. 7: Configuration of a ring of rigid cylinders and initial random configurations of cylinders in a cloaked annulus around the object to be cloaked.

3.1. Cloak Design

In order to study the cloaking efficiency we consider two cases. In the first we minimize the TSCS at a fixed value of frequency while supplying the gradients \mathbf{s}_j . In the second case we minimize the root mean square of a set of TSCS over a range of frequencies. In both cases, we supply the analytical formulas for the gradients of objective functions. The cost functions are non-convex with many local minima; we solve the non-convex optimization problems with non-linear constraints. For simplicity and demonstration of implementation of the proposed approach, we consider a configuration of uniform cylinders/shells of radius a.

3.1.1. Constraints

The constraints are as follows:

1. The cylinders are constrained to move inside a fixed cloaking annulus between the inner $r = R_i$ and outer $r = R_{out}$ boundaries surrounding the object being cloaked, see Figure 7.

Thus

$$R_i < |\mathbf{r}_i| < R_{out} \tag{3.21}$$

where $\mathbf{r_j} = (x_j, y_j)$ and $j = 1 + M_c, 2 + M_c, ..., M_a + M_c$; M_c is the total number of cylinders being cloaked, and M_a is the total number of cylinders in the annulus with $M_a + M_c = M$, M is the total number of cylinders.

2. In order to avoid overlapping the distance between the centers of cylinders/shells are constrained by

$$|\mathbf{r}_i - \mathbf{r}_i| > 2a + \delta$$
, with $a = 0.0075 \, m$, $\delta = 0.0005 \, m$. (3.22)

To avoid overlapping in cloak design, Andkjær and Sigmund ¹⁵ used the penalty function method with gradient-based topology optimization by penalizing the distance between the cylinders, i.e. adding the distance measure to the objective function as a penalty. Constrained problems can be approximated using penalty function methods that satisfy the constraints as well as use an unconstrained problem logic. Penalty function approaches are useful for incorporating constraints into derivative-free and heuristic search algorithms. However, here we use direct optimization methods such as Sequential Quadratic Programming (SQP) algorithms to get the best performance by taking advantage of the analytical form for the gradients of objective functions combined with parallel computing. In ³³, it is suggested to include a gradient evaluation in the objective function for faster or more reliable computations.

MATLAB build fmincon solver is a nonlinear programming solver that finds a local minimum of constrained nonlinear multivariable function. The fmincon interior-point and SQP algorithms ³³ work with both constraints, however, in our simulations, the interior-point algorithm produced less accurate results than SQP. Therefore, here we use the SQP method ^{34,35} as it provides more efficient and accurate result. The SQP is widely used in engineering applications and has fast convergence for many problems. The SQP algorithms represent the state of the art in non-linear programing methods. They are considered to be one of the best gradient-based algorithms ³⁵. Schittkowski found ³⁶ the SQP methods to require fewer function and gradient evaluations and outperform many other methods in terms of efficiency, accuracy, and percentage of successful solutions for a large number of test problems.

The closest proximity according to the constraint (3.22) should be far greater than the viscous skin depth $\delta_v = (2\nu/\omega)^{1/2}$. ³⁷ In water, at temperature $T = 5^oC$ with kinematic viscosity $\nu = 1.5182mm^2/s$, ³⁸ this is $\delta_v = \frac{0.000695m/\sqrt{s}}{\sqrt{f}}$ for frequency f (Hz); hence the undamped acoustic model is accurate for frequencies in kHz and above, which is the range of practical interest.

3.1.2. Broadband Cloak Design

The procedure for a broadband gradient based optimization is as follows. First, we define the cost function as the root mean square (RMS) of a set of TSCSs over some range of normalized wavenumbers $k_i a (i = 1, 2, ..., N_k)$:

$$\sigma_{RMS}(\mathbf{r}_{jm}) = \left(\frac{1}{N_k} \left[\left(\sigma(k_1 a, \mathbf{r}_{jm}) \right)^2 + \left(\sigma(k_2 a, \mathbf{r}_{jm}) \right)^2 + \dots + \left(\sigma(k_{N_k} a, \mathbf{r}_{jm}) \right)^2 \right] \right)^{1/2}. \quad (3.23)$$

Then, we define the broadband gradient vectors with respect to positions \mathbf{r}_i

$$\mathbf{q}_{j} = \frac{\partial \sigma_{RMS}(\mathbf{r}_{jm})}{\partial \mathbf{r}_{j}}, \quad j = 1, 2, \dots M,$$
(3.24)

which can be found in terms of the individual single frequency gradients as

$$\mathbf{q}_{j} = \frac{1}{\sigma_{RMS}} \frac{1}{N_{k}} \left[\sigma(k_{1}a)\mathbf{s}_{j}(k_{1}a) + \sigma(k_{2}a)\mathbf{s}_{j}(k_{2}a) + \dots + \sigma(k_{N_{k}}a)\mathbf{s}_{j}(k_{N_{k}}a) \right], \tag{3.25}$$

where $\mathbf{s}_{i}(k_{i}a)$ are evaluated at normalized wavenumbers $k_{i}a$ $(i = 1, 2, ..., N_{k})$.

A similar approach can be applied to minimizing the RMS of TSCS over a range of incident angles. However, in this case, the formula for the TSCS using the optical theorem, eq. (2.7), needs to be modified to become angle-dependent. This aspect will be studied elsewhere.

3.2. Numerical examples of acoustic cloaking

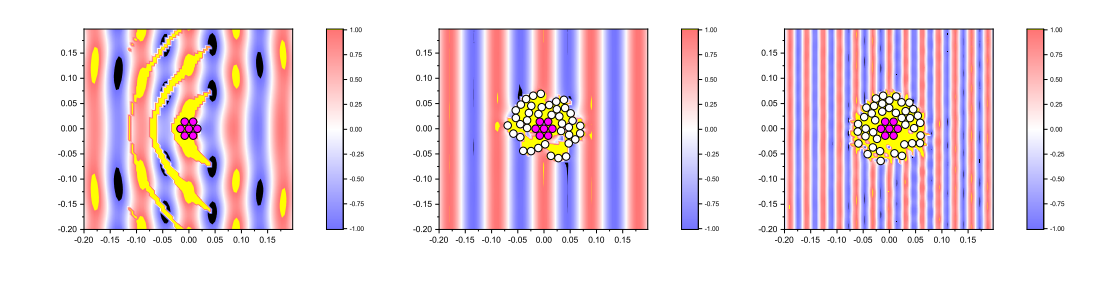


Fig. 8: The real part of the total acoustic pressure p_{total} a for a core of 7 rigid cylinders of radii a = 0.0075m without (a) and with (b,c) an optimized annular cloaking ring of 40 rigid cylinders. bNote that in this and the following figures σ_r is the normalized TSCS $\sigma_r = \sigma_{\text{with cloak}}/\sigma_{\text{without cloak}}$.

(a) No cloak: $\sigma = 0.12595$ (b) $ka = 0.525, \sigma_r = 1.4106e - 04$ (c) $ka = 1.5, \sigma_r = 0.0126$

Numerical results are demonstrated using MATLAB for configurations of rigid cylinders and empty thin elastic nickel cylindrical shells of thickness h=0.1a with mechanical properties: $\rho=8850~{\rm kg/m^3},~c_p=5480~{\rm m/s}$ where a is the outer radius. We consider cylinders and shells submerged in a medium with the acoustic properties of water: $\rho_0=1000~{\rm kg/m^3},~c_0=1480~{\rm m/s}$. All computations are for a plane wave incident from left to right.

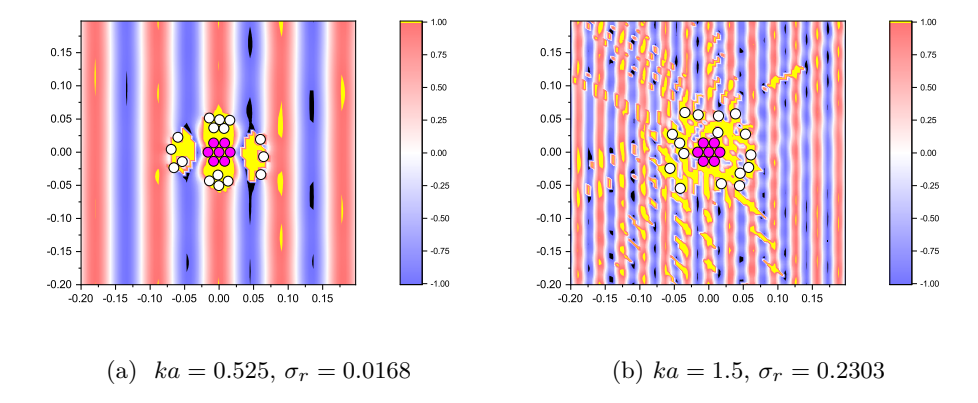


Fig. 9: Real part of total acoustic pressure field at different values of non-dimensional wavenumber $ka=0.525,\,1.5,\,$ for a ring of 7 rigid cylinders with an optimized annular cloak of 16 cylinders .

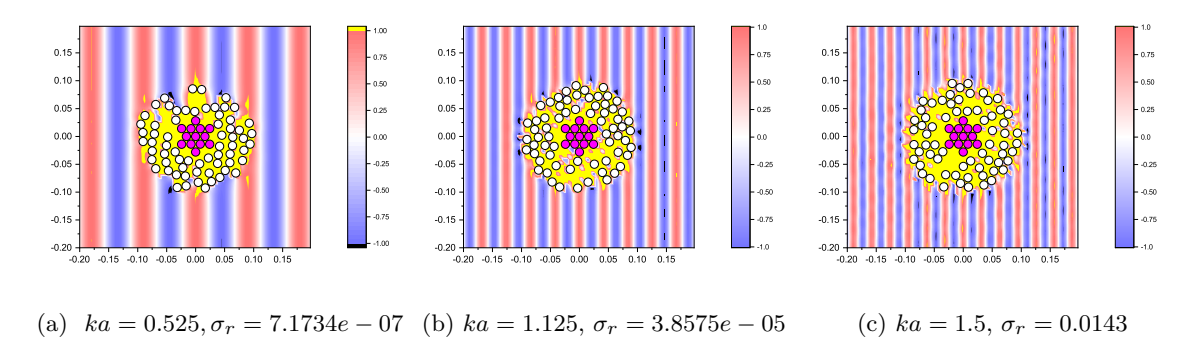


Fig. 10: Real part of total acoustic pressure field at different values of non-dimensional wavenumber ka=0.525, 1.125, and 1.5, for M=79: a multiring of $M_c=13$ rigid cylinders with an optimized annular cloak of $M_a=66$ cylinders .

In this section, we illustrate the effect of an exterior annulus cloaking device on plane wave scattering from a ring of cylinders/shells. In Figures 8 through 9, and 12 and 13, the object to cloak is a ring of $M_c=7$ identical rigid cylinders or thin shells of radii a=0.0075m centered at the origin shown in Figure 7(a). To show the efficiency of cloaking for larger objects, we consider a multiring configuration of $M_c=13$ rigid cylinders in Figures 10 and 11. Note that in all these figures: Figures 8 through 9, and then 11 through 13, σ_r is the normalized TSCS

$$\sigma_r = \frac{\sigma_{\text{with cloak}}}{\sigma_{\text{without cloak}}}.$$
(3.26)

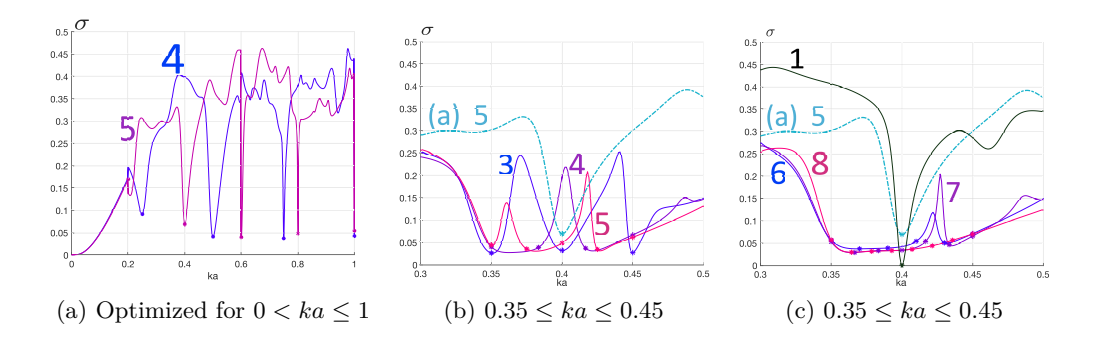


Fig. 11: A broadband cloak optimization is performed for the configuration of Figure 10. The numbers beside the curves indicate how many discrete frequencies employed, $N_k = \overline{1, 8}$. The range of normalized wavenumbers considered is 0 < ka < 1 in (a), and $0.35 \le ka \le 0.45$ in (b) and (c). The stars, *, denote minimum values of σ for different values of N_k . In (b) and (c), the dashed light blue curve "(a) 5" shows the enlarged view of curve with $N_k = 5$ from subfigure (a).

Various values are taken for the non-dimensional wavenumber, ka, the total number of scatterers, M, the number of scatterers in the cloaking annulus, M_a , and the number of discrete frequency points N_k for broadband cloaking as defined in eq. (3.23). Greater accuracy is observed, as expected, with increased number of scatterers M_a . However, large values of ka and M_a require longer computation times, and some numerical experimentation is necessary to find the smallest values for which the pressure field vanishes to the desired degree in the cloaked annulus.

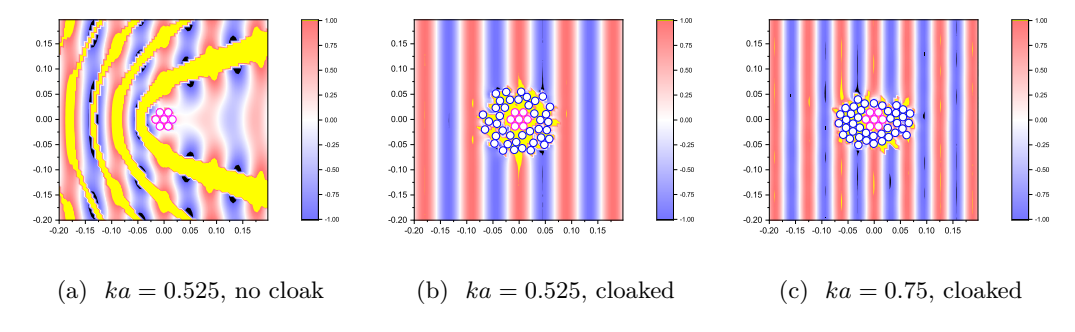


Fig. 12: The real part of the total acoustic pressure field p_{total} for a ring of 7 empty nickel thin cylindrical shells of thickness a/10 in water: without cloak, $\sigma=0.13447$ (a), and with an annular cloak of 40 similar cylinders at ka=0.525: $\sigma_{rel}=2.6436e-05$ (b) and $ka=0.75\sigma_{rel}=0.0018$ (c).

a MultiStart optimization solver, and supplying the gradients of TSCS with respect to position vectors. We start with an initial random planar configuration of rigid cylinders of uniform size, and radius a = 0.0075m, e.g. as shown in Figures 7(b)-7(c), and use MATLAB build function fmincon with MultiStart and the derived equations for the TSCS gradient, eq. (2.16). MultiStart has efficient local solvers, and can search a wide variety of start points in parallel. Providing the analytical gradients of the TSCS improves the optimized solution accuracy, reduces run time, and enables parallel computing using MultiStart. If the gradients are not supplied then fmincon estimates the derivatives using finite difference schemes which can be evaluated in parallel. But parallelization can be done only at one level: either at the outermost loop running MultiStart for different starting points or at the outermost parfor loop running fmincon and estimating gradients in parallel. Therefore, providing the gradients saves computational time, and can lead to increased accuracy. In addition, for constrained problems like the one considered here, providing a gradient has another advantage. As mentioned in fmincon documentation ³³: "a solver can reach a point x such that x is feasible, but finite differences around x always lead to an infeasible point. In this case, a solver can fail or halt prematurely. Providing a gradient allows a solver to proceed." Therefore, supplying the gradients accelerates the optimization process by searching a wide variety of start points in parallel and allows the solver to reach the optimum values which may otherwise be impossible. Here we present results for a ring configuration of $M_c = 7$ cylinders running 200 different random configurations concurrently on 8 CPUs of workstation. Computations for a multiring configuration of $M_c = 13$ cylinders were performed concurrently on 12 CPUs running 12, 36, or 100 scenarios (random configurations), described next.

3.2.1. Cloak design using rigid cylinders

Figures 8 through 10 show the cloaking effect for plane wave incidence on a core of rigid cylinders (the scatterer). The optimized cloak in each instance is an annular ring of similar rigid cylinders surrounding the core. The Figures consider various combinations of frequency ka and number of cylinders in the cloaking annulus. Figure 8 considers an annulus of 40 cylinders cloaking a core of 7 cylinders. It is noticed that cloaking performance diminishes with increase of frequency. This can be improved by increasing the number of cloaking cylinders and also by extending the outer radius of the cloaking annulus to allow the cylinders to explore a larger area, leading to faster convergence of the constrained optimization problem. A smaller number of cloaking cylinders, 16, is considered in Figure 9. This leads to more evident decrease in cloaking effectiveness at higher frequency. A larger cloaked object is considered in Figure 10: a core of 13 rigid cylinders, with a cloaking annulus of $M_a = 66$ cylinders. Figure 10 (c) depicts the results for ka = 1.5 when the size of a configuration is around two wavelength which is of similar size to the scatterer considered in ¹⁵; in this case the TSCS is of order 10^{-3} . The cloaking performance here can be improved by adding more cylinders in the cloaking annulus and increasing the size of the annulus. The design could be further enhanced by considering the cylinder radii as an additional design parameter. This requires deriving the gradients of TSCS with respect to the cylinder radii and will be studied elsewhere.

Figure 11 illustrates broadband cloaking performance. We optimize σ_{RMS} defined by eq. (3.23) for a given set of normalized wavenumbers $N_k = \overline{1, 8}$ while supplying the derived analytic form of the gradients \mathbf{q}_i from eq. (3.24). The results for $N_k = 4, 5$ in subfigure 11(a) consider a relatively wide frequency range: $0 < ka \le 1$ range. For instance, in Figure 11(a) for $N_k = 5$, σ is optimized for ka = 0.2, 0.4, 0.6, 0.8 and 1.0. The resulting TSCS is indeed reduced at the individual frequencies, but the overall TSCS still exhibits large values in the frequency range considered. This suggests that the frequency range is too ambitious for the small number of of discrete frequencies considered, and we therefore narrow it down to concentrate on a bandwidth around ka = 0.4. Subfigures 11(b) and 11(c) show results for $N_k = \overline{3,8}$ for the narrower interval $0.35 \le ka \le 0.45$ which corresponds to frequencies from 11 kHz to 14.1 kHz. It is evident from subfigures 11(b) and 11(c) that the cloaking performance range broadens with increasing N_k , and the peaks are smoothed out at $N_k = 8$. Interestingly, subfigure 11(c) indicates reduced TSCS values outside the optimized range of frequencies. Note that the TSCS is $\sigma = 4.6095e - 04$ when optimized at the single frequency $N_k = 1$: ka = 0.4, the black curve in Figure 11 (c). The tradeoff between the increase of the frequency band and cloaking efficiency leads to a reduced peak performance for broadband cloaking.

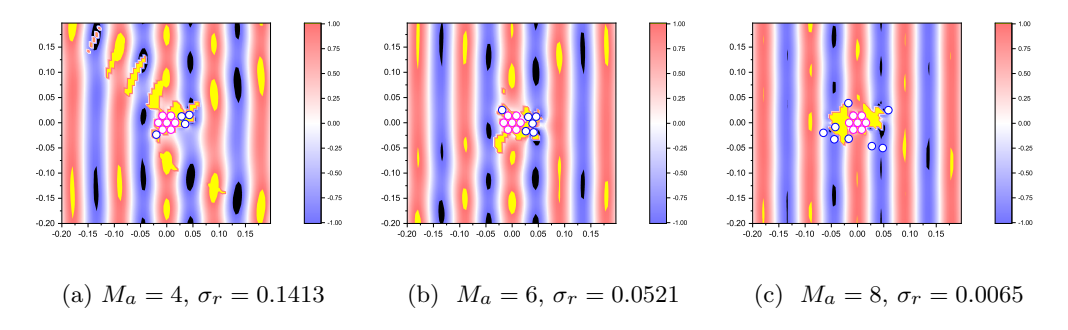


Fig. 13: The effect of increasing the number of number of thin cylindrical shell scatterers, M_a , in the annular cloak around a set of 7 central cylinders in water. The plots show the real part of total acoustic pressure at ka = 0.525.

3.2.2. Cloak design using thin elastic cylindrical shell

Finally, we illustrate the cloaking mechanism for thin cylindrical shells in water. This type of scatterer is quite different than the rigid cylinder because it can display large scattering effects at low frequency due to internal resonances of extensional and flexural waves. The thin shells considered have outer radii a=0.0075m, thickness h=a/10, with mechanical properties of nickel, $c_p=4.6e3$, $\rho_{sh}=8.90e3$, and the properties of water are $\rho_o=1e3$, $c_o=1.48e3$.

Figure 12 compares the response from a ring of 7 thin nickel shells with and without a cloaking annulus of 40 shells at two frequencies. The effectiveness of the cloak is obvious from the plots, and also from numerical values of the TSCS, e.g. at ka = 0.75 it is $\sigma = 0.116$ without the cloak, and $\sigma = 2.03e - 4$ when the cloaking device is on. Figure 13 displays the effect of varying the number of scatterers $M_a = 4$, 6, 8, in the cloaking annulus, showing how cloaking performance is enhanced with more scatterers. Note that the optimized cloaking configurations are not symmetric and do not completely surround the object being cloaked. This is advantageous from a practical point of view; the object being cloaked can be easily moved in or out of cloaking region.

4. Conclusions

The analytical form of the gradients of TSCS with respect to the cylinder positions are derived by means of MS theory and the optical theorem. As application of the method, a directional acoustic cloak is designed using a gradient based optimization method explicitly using the analytical formulas for the gradients of TSCS. Starting from a random spatial distribution, the cylinder positions are relocated in the process of minimizing the TSCS. The scatterer locations are optimized such that their combined scattering pattern cancel the scattering from a core (fixed) configuration of cylinders located inside the cloaked region. here we have examined acoustic MS from 2D cylindrical structures, although the method may be extended to 3D including elastodynamic ³² or electromagnetic material properties. The numerical results provide a means to establish realistic strategies for practical underwater applications. One area for consideration is the low-frequency range. The numerical simulations presented in this paper indicate that a small number of scatterers provide adequate cancellation at low frequencies. Cloaking performance can be improved by increasing the number of scatterers in the cloaking annulus as well as by increasing the size of the annular region at higher frequencies.

5. Acknowledgments

ANN acknowledges the support of the Office of Naval Research under MURI Grant No. N00014-13-1-0631. FAA acknowledges the support of the National Science Foundation under MRI CMMI Grant No. 1920363. The authors thank S. Bashash for a useful discussion on multi-variable optimization.

Appendix

A. Multiple Scattering Formulation

Consider acoustic scattering by M obstacles, which for simplicity are taken to be cylinders S_m , $(m = \overline{1, M})$ centered at \mathbf{r}_m . A schematic configuration of cylindrical elastic shells is given in Fig. 1. The incident wave of unit amplitude in direction $\mathbf{e}_1 = (1, 0)$ in the neighborhood

of cylinder S_m is

$$p_{inc}^{(m)}(\mathbf{x}) = \sum_{n=-\infty}^{\infty} A_n^{(m)} U_n^+(\mathbf{x}_m),$$
 (A.1)

with the coefficients $A_n^{(m)} = i^n e^{ikx_m}$ and $U_n^+(\mathbf{x}) = J_n(k|\mathbf{x}|)e^{in\arg\mathbf{x}}$, are the regular solutions associated with the radiating functions V_n^+ of (2.19). Also, $\arg\mathbf{x} \in [0, 2\pi)$, and \mathbf{x}_m is a position vector of point P with respect to the centers of multipoles at O_m (see Figure 1):

$$\mathbf{x}_m = \mathbf{x} - \mathbf{r}_m. \tag{A.2}$$

The total scattered field p_{sc} , considered as a superposition of the fields scattered by all cylinders, may be expanded as a sum of multipoles:

$$p_{sc}(\mathbf{x}) = \sum_{m=1}^{M} p_{sc}^{(m)}(\mathbf{x}), \quad p_{sc}^{(m)}(\mathbf{x}) = \sum_{n=-\infty}^{\infty} B_n^{(m)} V_n^+(\mathbf{x}_m),$$
 (A.3)

where $p_{sc}^{(m)}$ is the wave scattered by cylinder m, and $B_n^{(m)}$ are unknown coefficients. In order to apply boundary conditions on the surface of each cylinder we express the total field using Graf's theorem ³⁹:

$$V_l^+(\mathbf{x} - \mathbf{y}) = \sum_{n = -\infty}^{\infty} \begin{cases} V_n^+(\mathbf{x}) U_{n-l}^-(\mathbf{y}), & |\mathbf{x}| > |\mathbf{y}|, \\ U_n^+(\mathbf{x}) V_{n-l}^-(\mathbf{y}), & |\mathbf{x}| < |\mathbf{y}|, \end{cases}$$
(A.4)

where $U_n^-(\mathbf{x}) = J_n(k|\mathbf{x}|)e^{-\mathrm{i}\,n\arg\mathbf{x}} = (-1)^nU_{-n}^+(\mathbf{x})$ and $V_n^-(\mathbf{x}) = H_n^{(1)}(k|\mathbf{x}|)e^{-\mathrm{i}\,n\arg\mathbf{x}} = (-1)^nV_{-n}^+(\mathbf{x})$. The U_n^\pm and V_n^\pm functions therefore satisfy

$$W_n^+(\mathbf{x}) = W_{-n}^-(-\mathbf{x}), \quad W = U, \ V.$$
 (A.5)

Let $\mathbf{r}_{jm} = \mathbf{r}_j - \mathbf{r}_m$ be a position vector of multipole O_m with respect to multipole O_j . Since $\mathbf{x} = \mathbf{r}_m + \mathbf{x}_m = \mathbf{r}_j + \mathbf{x}_j \Rightarrow \mathbf{x}_m = \mathbf{x}_j + (\mathbf{r}_j - \mathbf{r}_m)$, the total field in the neighborhood of cylinder \mathbf{S}_j can be written as

$$p = \sum_{n=-\infty}^{\infty} \left\{ A_n^{(j)} U_n^+(\mathbf{x}_j) + B_n^{(j)} V_n^+(\mathbf{x}_j) + \sum_{\substack{m=1\\m\neq j}}^M B_n^{(m)} V_n^+(\mathbf{x}_j + \mathbf{r}_{jm}) \right\}.$$
 (A.6)

Then using Graf's theorem, we obtain for $|\mathbf{x}_j| < l_j$, where $l_j = \min |\mathbf{r}_{jm}|$:

$$p = \sum_{n=-\infty}^{\infty} \left[A_n^{(j)} U_n^+(\mathbf{x}_j) + B_n^{(j)} V_n^+(\mathbf{x}_j) + \sum_{\substack{m=1\\m\neq j}}^M B_n^{(m)} \sum_{l=-\infty}^{\infty} U_l^+(\mathbf{x}_j) V_{l-n}^-(\mathbf{r}_{mj}) \right]$$

$$= \sum_{n=-\infty}^{\infty} \left\{ B_n^{(j)} V_n^+(\mathbf{x}_j) + A_n^{(j)} U_n^+(\mathbf{x}_j) + U_n^+(\mathbf{x}_j) \sum_{\substack{m=1\\m\neq j}}^M \sum_{l=-\infty}^{\infty} P_{nl}(\mathbf{r}_{jm}) B_l^{(m)} \right\}, \quad (A.7)$$

where $P_{nl}(\mathbf{x})$, defined in (2.14), can be identified as $V_{l-n}^+(\mathbf{x})$. Here the matrix $\mathbf{P} = [P_{nl}]$ is equal to the transpose of Martin's $\mathbf{S} = [S_{nl}]$ matrix ⁴⁰. The total incident field impinging on the cylinder \mathbf{S}_i is a sum of the last two terms on the right hand side of eq. (A.7), i.e

$$p_{inc}^{(j)} + \sum_{\substack{m=1\\m\neq j}}^{M} p_{sc}^{(m)} = \sum_{n=-\infty}^{\infty} \left\{ A_n^{(j)} + \sum_{\substack{m=1\\m\neq j}}^{M} \sum_{l=-\infty}^{\infty} P_{nl}(\mathbf{r}_{jm}) B_l^{(m)} \right\} U_n^+(\mathbf{x}_j). \tag{A.8}$$

The response of cylinder S_j to the incident field (A.8) can be obtained by incorporating the boundary conditions at the interface and the transition matrix elements $T_{nq}^{(j)}$ of cylinder $S_j^{41,42}$:

$$p_{sc}^{(j)} = \sum_{n=-\infty}^{\infty} \sum_{q=-\infty}^{\infty} T_{nq}^{(j)} \left\{ A_q^{(j)} + \sum_{\substack{m=1\\m\neq j}}^{M} \sum_{l=-\infty}^{\infty} P_{ql}(\mathbf{r}_{jm}) B_l^{(m)} \right\} V_n^+(\mathbf{x}_j).$$
 (A.9)

Equations (A.3) and (A.9) yield a linear system of equations

$$B_n^{(j)} - \sum_{q=-\infty}^{\infty} T_{nq}^{(j)} \sum_{\substack{m=1\\m\neq j}}^{M} \sum_{l=-\infty}^{\infty} P_{ql}(\mathbf{r}_{jm}) B_l^{(m)} = \sum_{q=-\infty}^{\infty} T_{nq}^{(j)} A_q^{(j)}, \quad n \in \mathbb{Z}.$$
 (A.10)

Equivalently,

$$\sum_{q=-\infty}^{\infty} T_{nq}^{(j)-1} B_q^{(j)} - \sum_{\substack{m=1\\m\neq j}}^{M} \sum_{l=-\infty}^{\infty} P_{nl}(\mathbf{r}_{jm}) B_l^{(m)} = A_n^{(j)}, \quad n \in \mathbb{Z},$$
(A.11)

where $T_{nq}^{(j)-1}$ are elements of the inverse of the j^{th} T-matrix. Finally, we arrive at a system of equations for the unknowns $B_l^{(m)}$,

$$\sum_{m=1}^{M} \sum_{l=-\infty}^{\infty} X_{jnml} B_l^{(m)} = A_n^{(j)}, \quad j = \overline{1, M}, \quad n \in \mathbb{Z},$$
(A.12a)

$$X_{jnml} = \begin{cases} T_{nl}^{(j)^{-1}}, & j = m, \\ -P_{nl}(\mathbf{r}_{jm}), & j \neq m. \end{cases}$$
 (A.12b)

The truncated version of the infinite sum in equation (A.12a) yields a finite algebraic system of equations:

$$\sum_{m=1}^{M} \sum_{l=-N}^{N} X_{jnml} B_l^{(m)} = A_n^{(j)}, \quad j = \overline{1, M}, \quad n \in (-N, N),$$
(A.13)

or in matrix form

$$X \mathbf{b} = \mathbf{a}, \tag{A.14}$$

where \mathbb{X} , **b**, and **a** are given by eqs. (2.9) and (2.12).

Finally, the scattered field p^{sc} of eq. (A.3) in the far-field, $k|\mathbf{x}| \gg 1$, becomes

$$p^{sc} = f(\theta) \sqrt{\frac{k}{i 2\pi |\mathbf{x}|}} e^{i k|\mathbf{x}|} \left[1 + O\left(\frac{1}{k|\mathbf{x}|}\right) \right], \tag{A.15}$$

where the far-field amplitude function is

$$f(\theta) = \frac{2}{k} \sum_{m=1}^{M} e^{-i k |\mathbf{r}_m| \cos(\theta - \arg(\mathbf{r}_m))} \sum_{n=-\infty}^{\infty} (-i)^n B_n^{(m)} e^{i n\theta}.$$
 (A.16)

References

- 1. H. Chen and C. T. Chan. Acoustic cloaking in three dimensions using acoustic metamaterials. *Appl. Phys. Lett.*, 91(18):183518+, 2007.
- 2. S. A. Cummer and D. Schurig. One path to acoustic cloaking. New J. Phys., 9(3):45+, 2007.
- 3. A. N. Norris. Acoustic cloaking theory. Proc. R. Soc. A, 464:2411-2434, 2008.
- A. N. Norris, F. A. Amirkulova, and W. J. Parnell. Source amplitudes for active exterior cloaking. *Inverse Problems*, 28 (10) 105002, 2012.
- V. M. García-Chocano, L. Sanchis, A. Díaz-Rubio, J. Martínez-Pastor, F. Cervera, R. Llopis-Pontiveros, and J. Sánchez-Dehesa. Acoustic cloak for airborne sound by inverse design. *Appl. Phys. Lett.*, 99(7):074102+, 2011.
- L. Sanchis, V. García-Chocano, R. Llopis-Pontiveros, A. Climente, J. Martínez-Pastor,
 F. Cervera, and J. Sánchez-Dehesa. Three-dimensional axisymmetric cloak based on the cancellation of acoustic scattering from a sphere. *Phys. Rev. Lett.*, 110(12):124301+, Mar 2013.
- 7. Andreas Håkansson, Francisco Cervera, and JosSánchez-Dehesa. Inverse design of photonic crystal devices. *IEEE Journal on Selected Areas in Communications*, 23(7):1365 1371, 2005.
- 8. Andreas Håkansson, Francisco Cervera, and José Sánchez-Dehesa. Sound focusing by flat acoustic lenses without negative refraction. *Appl. Phys. Lett.*, 86:054102, 2005.
- 9. Andreas Håkansson, Daniel Torrent, Francisco Cervera, and José Sánchez-Dehesa. Directional acoustic source by scattering acoustical elements. *Appl. Phys. Lett.*, 90(22):224107, 2007.
- V. Romero-García, J. V. Sánchez-Péreza, L. M. García-Raff, J. M. Herrero, S. García-Nieto, and X. Blasco. Hole distribution in phononic crystals: Design and optimization. *Journal of the Acoustical Society of America*, 125:3774, 2009.
- 11. He Gao, Yi fan Zhu, Xu dong Fan, Bin Liang, Jing Yang, and Jian-Chun Cheng. Non-blind acoustic invisibility by dual layers of homogeneous single-negative media. *Scientific Reports*, 7(1):493740, feb 2017.
- 12. Alberto Serna, Luis J. Molina, Javier Rivero, Luis Landesa, and José M. Taboada. Multilayer homogeneous dielectric filler for electromagnetic invisibility. *Scientific Reports*, 8(1), sep 2018.
- 13. J. Andkjær and O. Sigmund. Topology optimized low-contrast all-dielectric optical cloak. *Appl. Phys. Lett.*, 98(2):021112, 2011.
- 14. J. Andkjær and O. Sigmund. Topology optimized acoustic and all-dielectric optical cloaks. In Photonic Crystals: Moulding the flow of lightroceedings of Metamaterials 2011: The Fifth International Congress on Advanced Electromagnetic Materials in Microwave and Optics, October 10-13 2011., October 10-13 2011.
- 15. J. Andkjær and O. Sigmund. Topology optimized cloak for airborne sound. *Journal of Vibration and Acoustics*, 135:041011, 2013.

- W. Lin, J.C. Newman III, and K. Anderson. Design of broadband acoustic cloak using topology optimization. In ASME IMECE Conference. Phoenix, AZ, pages IMECE2016–68135, 2016.
- 17. K. Diest, editor. Numerical Methods for Metamaterial Design, volume 127 of Topics in Applied Physics. Springer, 2013.
- S.R. Arridge and Martin Schweiger. A gradient-based optimization scheme for optical tomography. Optics Express, 2(6):213–226, 1998.
- 19. F. Amirkulova, S.T. Caton, M. Schrader, T.J. Gobel, and A. Norris. Acoustic gradient index lens design using gradient based optimization. *Journal of the Acoustical Society of America*, 143(3):1948–1948, 2018.
- 20. B. Blankrot and C. Heitzinger. Efficient computational design and optimization of dielectric metamaterial devices. https://arxiv.org/pdf/1804.09489.pdf, 2018.
- 21. L.S. Kalantari and M.H. Bakr. Wideband cloaking of objects with arbitrary shapes exploiting adjoint sensitivities. *IEEE Transactions On Antennas And Propagation*, 64(5):1963–1968, 05 2016.
- W. Chen, K. Diest, C. Kao, D. E. Marthaler, L. A. Sweatlock, and S. Osher. Gradient Based Optimization Methods for Metamaterial Design, volume 127, chapter Numerical Methods for Metamaterial Design. Topics in Applied Physics. Springer, Dordrecht, 2013.
- 23. H. Ronellenfitsch, N. Stoop, A. Forrow, and J. Dunkel. Designing spectral bandgaps in phononic networks. arXiv:1802.07214 [cond-mat.mtrl-sci], 2018.
- 24. I Peralta and V.D. Fachinotti. Optimization-based design of heat flux manipulation devices with emphasis on fabricability. *Scientific Reports*, 7: 6261, 2016.
- V.D Fachinotti and A. E. Peralta, I & Albanesi. Optimization-based design of an elastostatic cloaking device. Scientific Reports, 8:9857, 2018.
- C.A. Floudas and C. E. Gounari. A review of recent advances in global optimization. J. Glob. Optim., 45(1):3–38, 2009.
- 27. Seif-Eddeen K. Fateen and Adrián Bonilla-Petriciolet. Gradient-based cuckoo search for global optimization. *Mathematical Problems in Engineering*, 2014:1–12, 2014.
- 28. Ole Sigmund. On the usefulness of non-gradient approaches in topology optimization. *Structural and Multidisciplinary Optimization*, 43(5):589–596, mar 2011.
- 29. J Thomas, P. Gebraad, and A Ning. Improving the floris wind plant model for compatibility with gradient-based optimization. *Wind Engineering*, 41(5), 2017.
- 30. F. A. Amirkulova and A. N. Norris. Acoustic cloak by inverse design and gradient based optimization. *Journal of the Acoustical Society of America*, 142(4):2578–2578, 2017.
- 31. A. N. Norris. Acoustic integrated extinction. Proc. R. Soc. A, 471(2177):20150008+, Apr 2015.
- 32. F. A. Amirkulova. Acoustic and Elastic Multiple Scattering and Radiation from Cylindrical Structures. PhD thesis, Rutgers University, 2014.
- 33. MathWorks MATLAB Documentation. When the solver fails. https://www.mathworks.com/help/optim/ug/when-the-solver-fails.html.
- J. Nocedal and S. J. Wright. Numerical Optimization, Second Edition. Springer Series in Operations Research, Springer Verlag, 2006.
- 35. S. Rao. Engineering Optimization. Theory and Practice. John Wiley and Sons, Inc., 2009.
- K. Schittkowski. NLQPL: A FORTRAN-Subroutine Solving Constrained Nonlinear Programming Problems. Annals of Operations Research, 5:485–500, 1985.
- 37. Xiaoming Tang. Acoustic Logging in Fractured and Porous Formations. PhD thesis, MIT, 1990.
- 38. Viscosity Of Water. https://wiki.anton-paar.com/en/water/.
- M. Abramowitz and I. Stegun. Handbook of Mathematical Functions with Formulas, Graphs, and Mathematical Tables. Dover, New York, 1974.
- 40. P. A. Martin. *Multiple Scattering: Interaction of Time-harmonic Waves with N Obstacles*. Cambridge University Press, New York, 2006.

- 41. V. K. Varadan and V. V. Varadan, editors. Acoustic, Electromagnetic and Elastic Wave Scattering Focus on the T matrix Approach. Pergamon Press Inc, 1980.
- 42. F. A. Amirkulova and A. N. Norris. Acoustic multiple scattering using fast iterative techniques. In ASME 2017 IMECE, *Volume 13: Acoustics, Vibration and Phononics*,, 2017. Paper No. IMECE2017-72249, pp. V013T01A005; 10 pages.